ChemCatChem

Research Article
doi.org/10.1002/cctc.202501190

Chemistry Europe
European Chemical Societies Publishing

www.chemcatchem.org

Aerobic Cyclohexane Oxidation Catalyzed by Vanadium-Substituted $LaCoO_3$ Perovskites in the Liquid Phase

Akhil Hareendran,[a] Takuma Sato,[b] Leon Müller,[c] Anna Rabe,[d] Krishnan Ravi,[a] Dongsheng Zhang,[a] G. Wilma Busser,[a] Catalina Leiva-Leroy,[a] Heiko Wende,[d] Hartmut Wiggers,[c] Christof Schulz,[c] Alexander Schnegg,*[b] and Martin Muhler*[a, b]

Spray flame-synthesized $LaV_xCo_{1-x}O_3$ perovskites (x = 0.00, 0.01, 0.03, 0.05, 0.3, and 0.5) were found to enhance the KA oil (mixture of cyclohexanol and cyclohexanone) selectivity in the aerobic liquid-phase oxidation of cyclohexane. The KA oil selectivity significantly improved even for a low vanadium doping of x = 0.01, and for x = 0.03, conversion and KA oil yield reached 22.5% and 17.1%, respectively, under mild reaction conditions of 120 °C and 15 bar O_2. Kinetic investigations performed over $LaV_{0.03}Co_{0.97}O_3$ exhibited a first-order-like reaction with a low apparent activation energy of 44.8 kJ mol^{-1}, which is ascribed to the Co^{2+} fraction generated upon doping V, which decomposes the cyclohexyl hydroperoxide (CHHP) intermediate. Radical scavenging studies combined with the electron paramagnetic resonance (EPR) spin trap studies identified $C_6H_{11}OO^{\bullet}$, $C_6H_{11}O^{\bullet}$, $HO^{\bullet}$, $O_2^{\bullet-}$, and $C_6H_{11}^{\bullet}$ as the active free radicals. Post-reaction characterization revealed the partial reduction of Co^{3+} to Co^{2+} and presumably of V^{5+} to V^{4+} during cyclohexane oxidation. A plausible catalytic cycle is proposed based on an initial proton-coupled electron transfer (PCET) process where the higher-valent cations, such as Co^{3+} and V^{5+}, are reduced to lower-valent Co^{2+} and V^{4+}, which further participate in a Haber–Weiss cycle, decomposing the CHHP intermediate.

1. Introduction

The aerobic oxidation of cyclohexane provides an environmentally sustainable method to synthesize KA oil as opposed to traditional, less eco-friendly reactions.[1–3] Since the further oxidation of KA oil results in adipic acid, nylon-6,6 could be synthesized indirectly via cyclohexane oxidation.[4,5] Unfortunately, these processes are often associated with the use of toxic and non-ecofriendly oxidizing agents such as nitric acid.[6–8] Hence, alternative synthesis routes are of high relevance in an environmentally responsible society using molecular oxygen to oxidize traditional hydrocarbons with suitable catalysts.

The selective oxidation of cyclohexane is capable of generating KA oil, although this process is challenging due to the relatively lower stability of the product compared with cyclohexane.[9,10] The KA oil is easily oxidized to secondary products above specific conversion thresholds (Scheme 1). These byproducts often include diols, diones, carboxylic acids, and aldehydes. Therefore, maintaining steady KA oil selectivity is often challenging as C—H bond activation and breaking require high reaction temperatures.[11–14] A few attempts have been made to oxidize cyclohexane either solvent-free or by using homogeneous catalysts.[15–20] However, this reaction can also be carried out by using a suitable solvent and novel heterogeneous catalysts, resulting in significantly milder reaction conditions.[21–23]

La-based perovskites are reported to be efficient catalysts in hydrocarbon oxidation reactions.[24–26] Perovskites can be generally represented as ABO_3, where A and B are transition metals with different ionic radii. The A cation is usually larger than the B cation and often includes either lanthanides or alkaline metals. These sites can also be further partially substituted ($A_{1-x}A'_xB_{1-x}B'_xO_3$) to form mixed metal perovskites, thereby tuning their properties. One of these properties is the formation of oxygen vacancies that make them potential oxidation catalysts.[27–29] Some of these La-based perovskite catalysts are also reported to facilitate C—H bond activation and its breaking.[30–32] Further transition metal combinations have to be studied to design, develop, and predict the rational properties of potentially suitable catalysts. In particular, V as a dopant is recognized for its influence in promoting electron transfer processes in various cat-

[a] A. Hareendran, K. Ravi, D. Zhang, G. W. Busser, C. Leiva-Leroy, M. Muhler
Laboratory of Industrial Chemistry, Ruhr University Bochum, Universitätsstraße 150 44801, Bochum, Germany
E-mail: martin.muhler@ruhr-uni-bochum.de

[b] T. Sato, A. Schnegg, M. Muhler
Max Planck Institute for Chemical Energy Conversion 45470, Mülheim an der Ruhr, Germany
E-mail: alexander.schnegg@cec.mpg.de

[c] L. Müller, H. Wiggers, C. Schulz
Institute for Energy and Materials Processes– Reactive Fluids, University of Duisburg-Essen 47057, Duisburg, Germany

[d] A. Rabe, H. Wende
Faculty of Physics and Center for Nanointegration Duisburg-Essen (CENIDE), University of Duisburg-Essen, Duisburg 47057, Germany

Supporting information for this article is available on the WWW under https://doi.org/10.1002/cctc.202501190

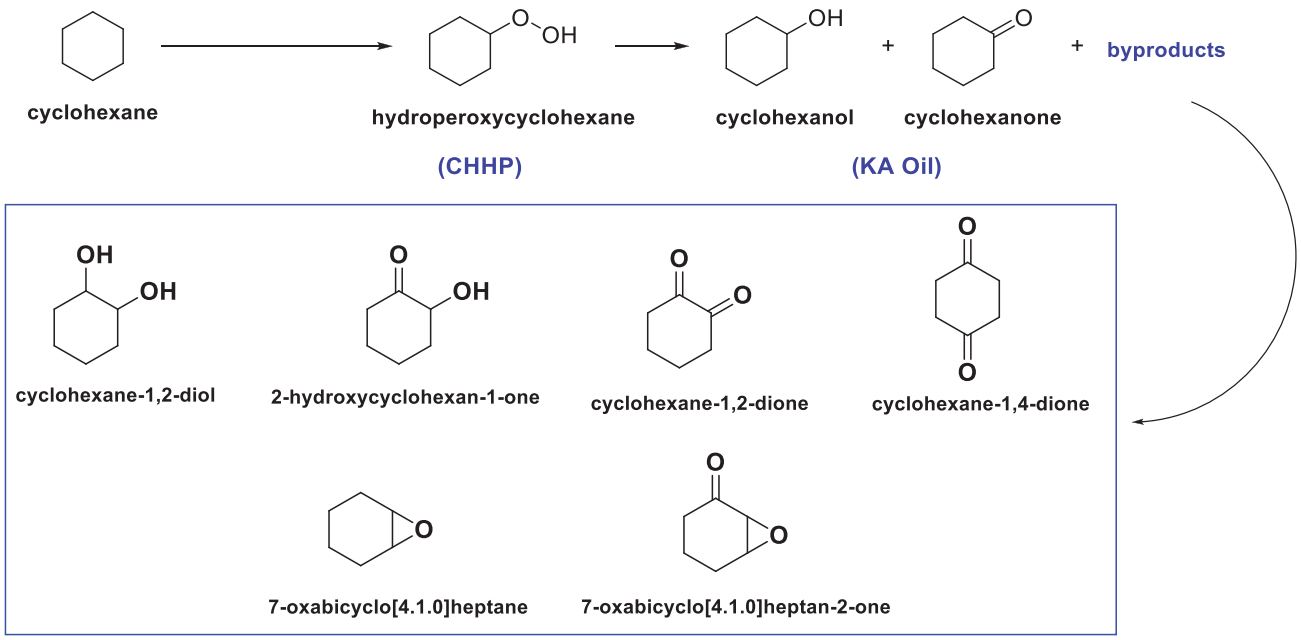

Scheme 1. Reaction network of cyclohexane oxidation.

alytic systems, including the oxygen evolution reaction.[33–35] This showcases the scope of V as a potential dopant in hydrocarbon oxidation reactions that involve proton-coupled electron transfer (PCET).[25]

One of the missing factors is to link the catalytic structure to the selectivity distribution. With free radicals being the active species, the catalyst could also play a crucial role in selectively maintaining their population.

Currently, there is a lack of mutual correlations between catalytic structure, radical population, and product selectivity in order to effectively identify the catalytic properties in perovskites. Therefore, a thorough temporal monitoring of the catalytic structure and the free radicals during the reaction is a leap forward in understanding heterogeneously catalyzed cyclohexane oxidation.

Herein, we report on the catalytic liquid-phase oxidation of cyclohexane over $LaV_xCo_{1-x}O_3$ perovskites, attempting to correlate structure, generated radicals, and product selectivity during cyclohexane oxidation. The positive effect of increasing the V content on catalytic performance was confirmed and systematically investigated through screening experiments. Kinetic investigations varying the initial cyclohexane concentration, reaction temperature, and O_2 pressure were carried out to study their impact on the reaction profile. Radical scavenging studies combined with spin trap electron paramagnetic resonance (EPR) spectroscopy studies facilitated the identification and quantification of the free radicals formed. In combination with these results, correlations were made with the KA oil and byproduct yields to gain insights into selectivity improvement in cyclohexane oxidation, supported by post-reaction characterization using techniques such as solid-state EPR, X-ray diffraction (XRD), X-ray photoelectron spectroscopy (XPS), H_2 temperature programmed reduction (TPR), and Raman spectroscopy under reaction conditions.

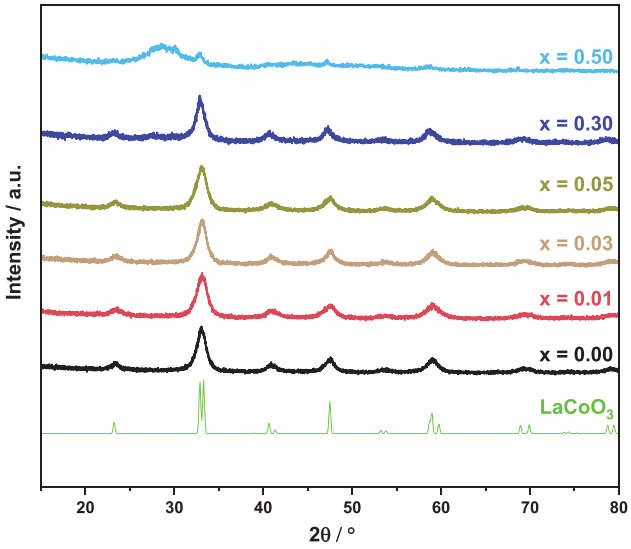

Figure 1. X-ray diffraction patterns of the as-synthesized $LaV_xCo_{1-x}O_3$ nanoparticles. Reference spectrum: ICSD 153993 (orthorhombic $LaCoO_3$).

2. Results and Discussion

2.1. Characterization of the As-Synthesized Catalysts

Figure 1a shows the XRD patterns of the spray flame-synthesized $LaV_xCo_{1-x}O_3$ nanoparticles, where "x" represents the V content in at%. In general, V^{5+} (0.54 Å) can be well incorporated into the perovskite lattice, since Co^{3+} (0.55 Å) has a similar ionic radius. The XRD patterns confirm the presence of an orthorhombic phase based on the reference pattern (ICSD: 153993). The perovskites are found to be phase-pure up to 5% V doping, and its further increase results in phase segregation as indicated by the very broad reflection around 28.78°. The reflections are relatively

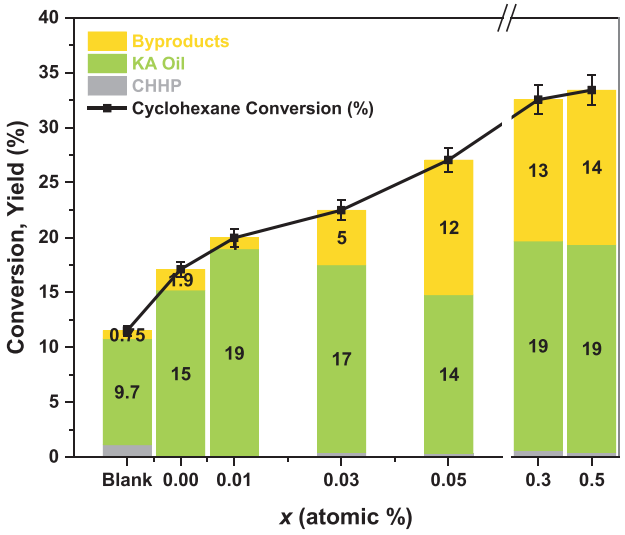

Figure 2. Conversion-yield profile of screening $LaV_xCo_{1-x}O_3$ for cyclohexane oxidation. Reaction conditions: 120 °C, 1.00 mol/L cyclohexane, 25 mg catalyst, 15 bar O_2, 600 rpm, and 6 h.

broad compared with those of the reference material, indicating low crystallinity. The cell parameters together with the crystallite sizes are summarized in Table S1. With rising V content the c-axis lattice parameter was found to be increasing indicating Co-O bond elongation. Doping V in the +5 oxidation state introduces excess positive charge, possibly leading to the generation of vacancies and/or Co^{2+}. The crystallite size amounted to about 10 nm except for x = 0.5. N_2 physisorption experiments were performed to derive the specific surface areas (BET equation) of the nanoparticles (Table S1) in the range from 80 to 110 m^2/g.

2.2. Catalytic Screening and Kinetic Investigations

The spray flame-synthesized $LaV_xCo_{1-x}O_3$ nanoparticles were applied in the liquid-phase oxidation of cyclohexane. Previous studies using Co-based perovskites as catalysts confirmed the positive influence in selective cyclohexane oxidation.[25] The substitution of V into $LaCoO_3$ may enhance the catalytic properties due to the generation of oxygen vacancies and/or Co^{2+}. The reaction was carried out based on our previous work, where cyclohexane was oxidized using molecular oxygen in acetonitrile at 120 °C.[25]

Owing to its relatively lower thermal stability, KA oil is easily further oxidized to secondary products such as shown in Scheme 1. These are mainly cyclohexane-1,2-diol, cyclohexane-1,2-dione, cyclohexane-1,4-diol, cyclohexane-1,4-dione, 2-hydroxycyclohexanone, and 7-oxabicyclo[4.1.0]heptan-2-one. Further oxidation could also lead to the formation of adipic acid or even CO_2, but this is not identified in this work. In reference to our previous work, the reaction parameters were set at 120 °C, 1.00 mol/L, 15 bar O_2, 600 rpm, and 6 h.[25]

Figure 2 shows the overall conversion-yield profile obtained with the $LaV_xCo_{1-x}O_3$ catalysts. A conversion of 11.5% was achieved for the uncatalyzed reaction after 6 h with 9.65% KA oil yield. The reaction profile of the individual catalysts is shown in Figure S1. As soon as $LaCoO_3$ (x = 0.00) was introduced, conversion increased to 17.1% with a higher KA oil yield of 15.2% and 1.9% of byproducts. The beneficial effects of $LaCoO_3$ as a catalyst for cyclohexane oxidation have already been reported in our previous work.[25] Compared with the uncatalyzed reaction, the cyclohexyl hydroperoxide (CHHP) intermediate was completely decomposed in the presence of $LaCoO_3$. Incorporating 1 at% of V into $LaCoO_3$ further enhanced conversion to 20%, and the V doping up to 3 at% yielded KA oil as the major product at an even higher degree of conversion with only 5% byproducts. Table S2 summarizes the corresponding product selectivities. The blank reaction is associated with the highest CHHP selectivity of 9% after 6 h. Upon adding $LaV_xCo_{1-x}O_3$, negligible amounts of CHHP (selectivity < 2%) were obtained. A high selectivity of KA oil (95%) was achieved for $LaV_{0.01}Co_{0.99}O_3$ at a relatively high conversion of 20%. Table S3 summarizes a comparison of this work with other studies on Co- and V-based catalytic cyclohexane oxidation.

For $LaV_{0.03}Co_{0.97}O_3$, 17.1% KA oil was obtained at a conversion of 22.5%. Even though further increments in V enhanced conversion, the undesired byproduct formation was significantly higher. Therefore, the role of the catalyst is to increase the conversion threshold up to which KA oil is still stable.[25] The byproduct yield increased up to 12% when the V content increased to 5 at%. At 50 at%, a conversion of 33.4% was obtained with 19% KA oil. The maximum KA oil yield of approximately 19% was also achieved for lower V contents of 1 and 3 at%. Thus, the higher V contents catalyze the reaction efficiently, leading to higher conversion, but do not enhance the KA oil selectivity.

Owing to its relatively higher conversion and appreciable V content, $LaV_{0.03}Co_{0.97}O_3$ was chosen for kinetic investigations. The standard reaction parameters were set as 130 °C, 15 bar O_2, 600 rpm, 6 h and 25 mg catalyst. A temperature of 130 °C in contrast to screening at 120 °C was chosen in correlation with the radical scavenging and EPR experiments, since the radical generation and detection were better at this temperature. The increase in conversion with increasing initial cyclohexane concentration is shown in Figure 3a. The cyclohexane concentration was varied as follows: 0.75, 0.85, 1.00, and 1.15 mol/L. A maximum KA oil yield of 25% was observed for a conversion of 32.1% at 1.15 mol/L. The KA oil yield is strongly dependent on the initial cyclohexane concentration, and optimizing its concentration can therefore facilitate to achieve the maximum KA oil selectivity at a particular reaction temperature. Figure 3b shows the linearized plot of the reaction rate as a function of the initial cyclohexane concentration. The linear regression of the plot reveals first-order reaction kinetics with respect to cyclohexane at a constant pressure of 15 bar O_2. The individual reaction profiles of the concentration variations are shown in Figure S2.

The conversion and yield after 6 h as a function of the reaction temperature is shown in Figure 3c. The reaction profile at each applied temperature is shown in Figure S3. The reaction at 110 °C resulted in a conversion of 10.8% with an induction period of 1 h (Figure S3). At 120 °C, the conversion increased to 22.5% with a KA oil yield of 17%. Traces of CHHP intermediate are also identified for both reactions after 6 h. A higher KA oil yield of

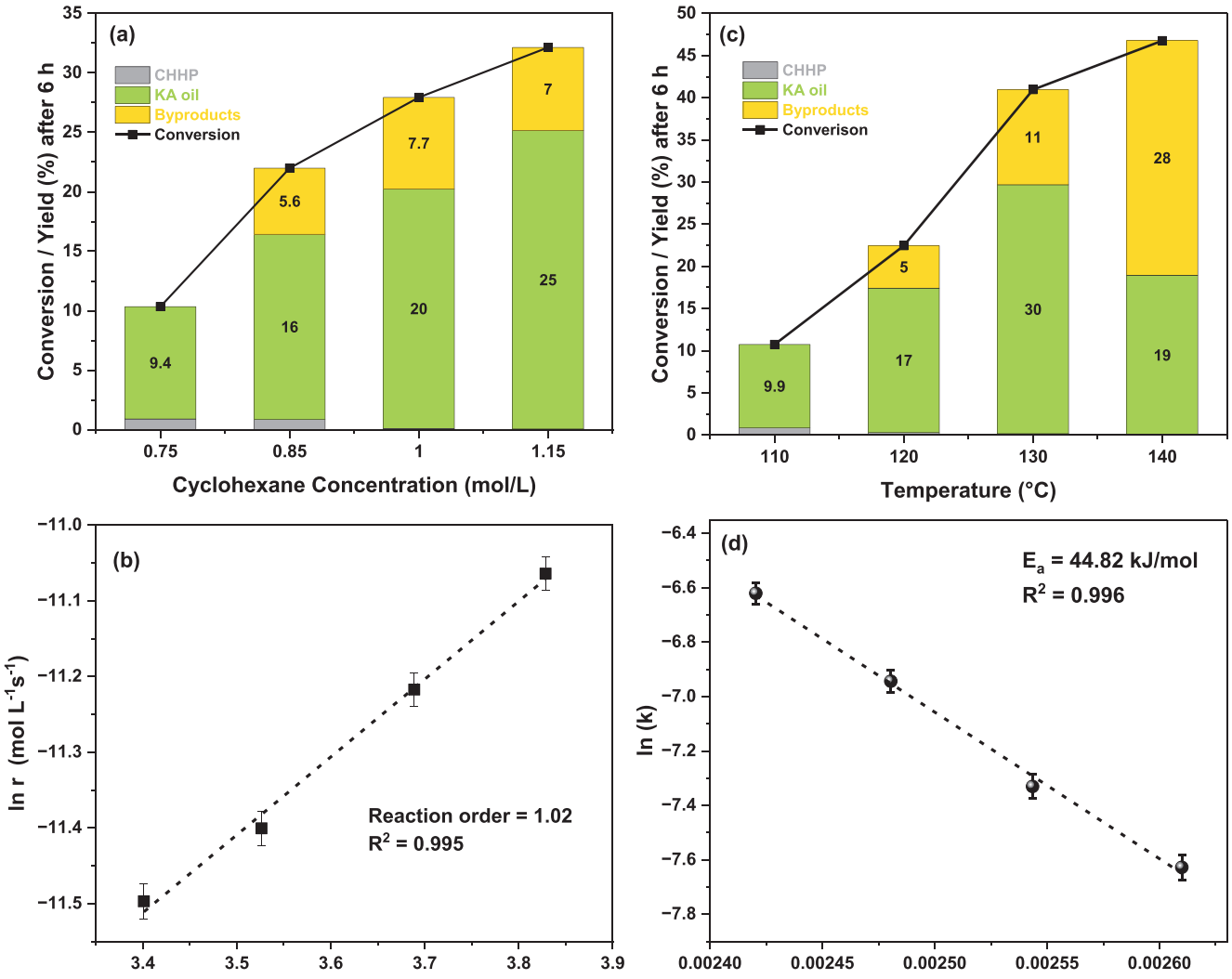

Figure 3. a) Effect of cyclohexane concentration on the conversion-yield profile, b) linearized plot of the reaction rate over $LaV_{0.03}Co_{0.97}O_3$ as a function of the initial cyclohexane concentration, c) effect of reaction temperature on cyclohexane oxidation, d) Arrhenius analysis based on first-order reaction kinetics. Optimized reaction conditions: 130 °C, 1.00 mol/L, 15 bar O_2, 25 mg $LaV_{0.03}Co_{0.97}O_3$, 600 rpm, and 6 h.

30% is obtained when the temperature is increased to 130 °C. The increase is associated with a higher degree of cyclohexane conversion (41%), where 11% byproducts are also obtained. Despite the conversion increase to 47%, the KA oil is significantly oxidized to byproducts at 140 °C. A lower KA oil yield of 19% and byproduct yield of 28% is obtained during the reaction at 140 °C. The temperature variation confirmed the dependence of KA oil stability on reaction temperature. This further supports our previous findings where KA oil is stable only up to a certain conversion threshold, depending on the catalyst.[25] Figure 3d shows the Arrhenius analysis based on the temperature variation experiments. The rate constants were derived based on first-order kinetics (Equation S2). An apparent activation energy of 44.8 kJ/mol is determined with high accuracy ($R^2 = 0.996$) under the applied reaction conditions.

Figure S4a shows the effect of O_2 pressure on cyclohexane oxidation over $LaV_{0.03}Co_{0.97}O_3$ using 5, 10, 15, and 20 bar. The pressure decrease to 5 bar resulted in a cyclohexane conversion of 40% with a 30.8% KA oil yield, confirming an increased reaction rate at lower O_2 pressure. This finding aligns with our previous studies, which demonstrated that increased O_2 pressure enhances the radical recombination rate, resulting in a lower degree of conversion.[25] At higher O_2 pressure, $C_6H_{11}OO^{\bullet}$ radicals are highly abundant, increasing the rate of termination.[36–38] External mass-transfer limitations were checked by varying the stirring speed of the reactor at 500, 600, and 700 rpm. As Figure S4b shows, the stirring speed did not significantly influence the conversion-yield profile of the reaction. Internal mass transfer limitations were absent as the synthesized nanoparticles were non-porous. The individual reaction profiles of the O_2 pressure and the stirring speed variations are shown in Figures S5 and S6.

The reusability of $LaV_{0.03}Co_{0.97}O_3$ as a catalyst was tested by using it in three consecutive reactions, as shown in Figure S7a. The conversion-yield profile remained comparable even after the three reaction cycles. Conversion remained between 26.7% and 27.2% with a KA oil yield of 19.3%–19.8% over the cycles. The structural integrity of the catalyst was confirmed by the XRD pattern after three reaction cycles (Figure S7b).

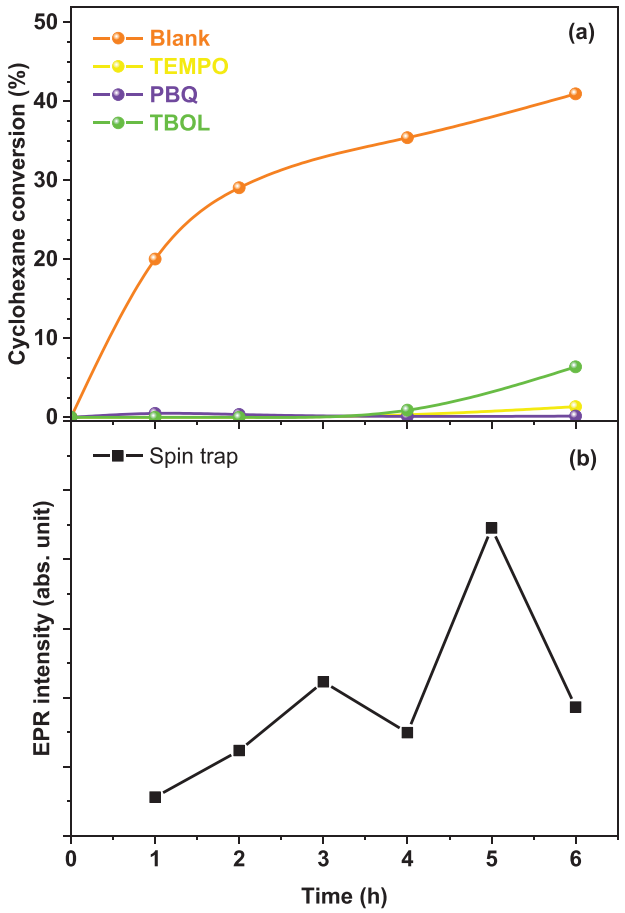

Figure 4. a) Cyclohexane conversion in the presence of different radical scavengers, b) radical amount determined as EPR intensity of DMPO adducts in solution, both plotted versus reaction time. Reaction conditions: 130 °C, 1.00 mol/L cyclohexane, 15 bar O_2, 600 rpm, 6 h, 2 mol% of radical scavenger, 25 mg $LaV_{0.03}Co_{0.97}O_3$.

2.3. Radical Scavenging and EPR Spin Trap Studies

To study the presence and influence of free radicals, scavenging experiments were performed using different radical scavengers. TEMPO ((2,2,6,6-tetramethylpiperidin-1-yl)oxyl) can be used to scavenge nearly all types of free radicals[39,40] and has been widely employed as a spin trap in EPR spectroscopy.[41] While peroxyl and superoxyl radicals can be scavenged using *p*-benzoquinone (PBQ), hydroxyl and alkoxyl radicals are scavenged using *tert*-butanol (TBOL).[42,43] The influence of the different radical scavengers on cyclohexane conversion is shown in Figure 4a. As a reference, the catalyzed reaction at 130 °C is included as the blank experiment (orange). The addition of both TEMPO and PBQ quenched the reaction leading to no observable conversion (<1%) even at the 6th h.

While scavenging using TEMPO confirmed free radicals as the active species during reaction, PBQ confirmed the significant influence of peroxyl radicals ($C_6H_{11}OO^{\bullet}$, $O_2^{\bullet-}$) in conversion. Although scavenging aimed at $C_6H_{11}O^{\bullet}$, $HO^{\bullet}$ using TBOL also has a similar effect till the 4th h, a conversion of about 6% is obtained at the 6th h. Despite this fluctuation at the 6th h, conversion is still significantly lower than for the blank experiment (41%). Therefore, it has to be concluded that both peroxyl and alkoxyl radicals significantly influence the conversion of cyclohexane. To monitor the individual radicals present during cyclohexane oxidation, spin trap studies using EPR spectroscopy were carried out. The spin trap 5,5-dimethyl-1-pyrrolin-*N*-oxide (DMPO) was added to the reaction solution to determine the radical amount present after different reaction times. Figure 4b shows the evolution of the integrated EPR signal directly proportional to the radicals present in the reaction solution after reaction times from 1 to 6 h with increments of 1 h. Although radicals may both originate directly from the reaction in the reactor or from autoxidation processes in the EPR tube, the number of trapped radicals after varying reaction times clearly differs. In the samples measured after 1, 2, and 3 h, the radical content of the solutions increases steadily, decreases at 4 h, and then reaches a value almost twice as high after 5 h as after 3 h. This time course correlates with a steep increase in the KA oil yield in cyclohexane oxidation in the first 3 h and a levelling off of the KA oil yield after 4 h. However, the time course and the shape of the EPR spectra (Figure S8) differ significantly from those in our recently published study on cyclohexane oxidation over Fe-substituted $LaCoO_3$.[25] Unlike in the latter case, cyclohexane oxidation over $LaV_{0.03}Co_{0.97}O_3$ seems to involve the formation of $O_2^{\bullet-}$ radicals over longer reaction times (>3 h) (see Figure S8), which appears to be accompanied by the increased production of byproducts. The mechanism behind this process is not yet understood and is currently the subject of further investigation.

2.4. TBHP Decomposition Over $LaV_{0.03}Co_{0.97}O_3$

An investigation on the catalytic ability to decompose the hydroperoxide intermediate was performed as shown in Figure S9a,b. Since CHHP is difficult to synthesize and stabilize, *tert*-butyl hydroperoxide (TBHP) was used as a model peroxide intermediate. The setup to measure the evolved O_2 during TBHP decomposition is shown in Figure S9a. The catalytic ability to decompose the hydroperoxide intermediate can then be related to the evolved O_2 volume. To study the catalytic influence on hydroperoxide decomposition, the thermal influence has to be kept minimal. The blank experiment performed at 50 °C confirmed a negligible effect of temperature on TBHP decomposition, as it yielded less than 0.5 mL O_2 even after 6 h. Upon introducing non-doped $LaCoO_3$, the evolved volume increased to about 7.2 mL at the 6th h. When $LaV_{0.03}Co_{0.97}O_3$ (fresh) was added, the volume further increased to 9.65 mL, confirming the beneficial effect of V as a dopant. Additionally, $LaV_{0.03}Co_{0.97}O_3$ after cyclohexane oxidation (spent) was also used to study its influence on hydroperoxide decomposition. Interestingly, the spent catalyst yielded a relatively higher O_2 volume of 10.8 mL after 6 h. Similar to our previous investigations, a potential surface change of the catalyst during cyclohexane oxidation has to be assumed to have occurred.[25] A possible explanation would be the reduction of the surface during cyclohexane oxidation, resulting in more exposed Co^{2+} sites. Advanced characterization techniques have to be employed to further understand the modified catalytic surface.

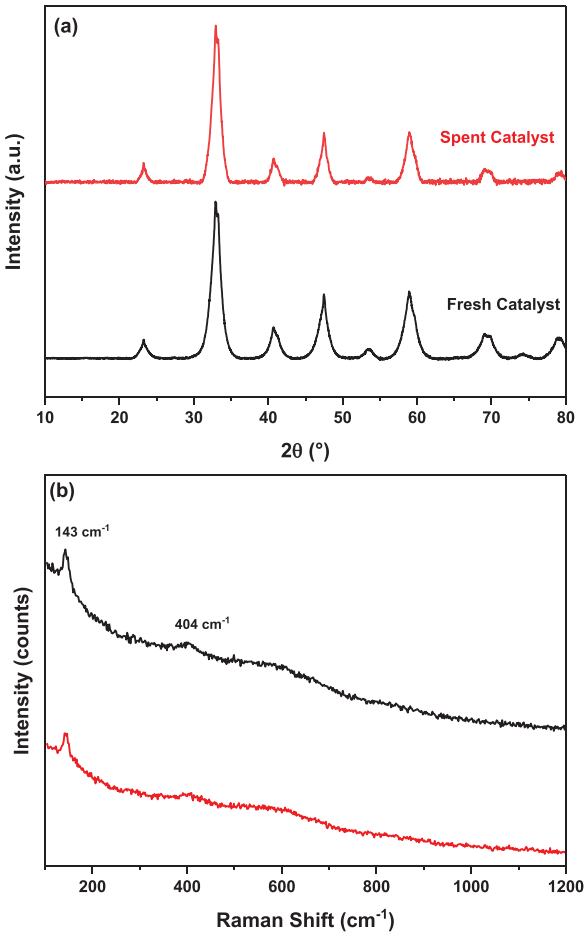

Figure 5. Characterization of the fresh and spent $LaV_{0.03}Co_{0.97}O_3$ nanoparticles after reusability studies using a) XRD and b) Raman spectroscopy.

2.5. Post-Reaction Characterization of $LaV_{0.03}Co_{0.97}O_3$

As shown in Figure 5a,b, the post-reaction XRD and Raman measurements confirmed the structural integrity of the catalyst being preserved during the reaction. The XRD patterns do not show any significant changes of the major peak characteristics in the spent catalyst with a relatively lower intensity at higher diffraction angles. The Raman spectra exhibited similar shifts for the catalysts before and after reaction, which correspond to those reported in literature.[44] The ICP-MS measurements after reaction further demonstrate the stability of the catalyst and are summarized in Table S4. The morphologies of the fresh and spent catalysts were studied using high-resolution transmission electron microscopy (HR-TEM) as shown in Figure S10. No significant changes related to the structure or morphology of the non-porous nanoparticles were observed, and the characteristic lattice fringes of 0.275 nm (100) were maintained, thereby further confirming the preservation of structural integrity.[45,46]

Figure 6a shows the EPR spectra of the fresh (black) and spent (red) $LaCo_{0.97}V_{0.03}O_3$ powder samples recorded at 15 and 298 K. In the fresh sample, a broad and asymmetric line with a maximum at an effective g value of $g^{eff} \sim 5.6$ was observed. This spectrum was assigned to high-spin (HS, $S = 3/2$) Co^{2+}.[47] No vanadium-related signal was detected in fresh samples, suggesting that the oxidation state of V is either 3+ or 5+ . In the spent sample, an increase in EPR intensity of the HS Co^{2+} signal was observed, as well as an emergence of V^{4+}. Although V^{4+} could be clearly identified by its characteristic EPR line shape,[48] quantification revealed that only a sub-percent fraction of the total vanadium content in the sample was in the paramagnetic V^{4+} state.

The changes in surface oxidation states were investigated using XPS. The Co 2p spectrum of the fresh and spent catalyst after normalization at 779.8 eV is shown in Figure 6b. The increase in the satellite intensities of the spent catalyst at 786.5 eV and at 804.2 eV confirms the reduction of Co^{3+} to Co^{2+} during cyclohexane oxidation. This is in line with the EPR results and our previous investigations, where Co-containing perovskites were found to undergo partial reduction during reaction to Co^{2+}.[25] The individual Co 2p spectra of the fresh and spent catalysts are shown in Figure S11. The peaks (green) at 779.1, 780.4, 782.2, and 789.2 eV are identified to originate from an octahedrally coordinated Co^{3+}-dominant system.[49] The Co^{2+} contributions (blue) are identified mainly in the spent catalyst at 779.6 eV, 781.4 eV, and 786 eV. The reduction of Co^{3+} (0.61 Å) to Co^{2+} (0.75 Å) facilitates the CHHP decomposition via the known Haber-Weiss reactions. The O 1s spectra of the fresh and spent catalysts in Figure S12 also show significant differences. The peaks appear mainly around 528.7 eV (lattice oxygen) and 531.0 eV (adsorbed hydroxyl groups). The relatively higher intensity at 531.0 eV for the spent catalyst further confirms the CHHP decomposition by Co^{2+}, where water is formed as a coupled product. Subsequent changes are also observed in the La 3d spectra (Figure S13), where the contribution at 835.5 eV is increased after reaction. The change in the fine splitting of La $3d_{5/2}$ spectra might further indicate local changes in oxidation state or electronic rearrangements. The changes in the C 1s spectra are shown in Figure S14, where higher oxygenate contributions are observed in the spent catalyst.

The H_2 TPR measurements shown in Figure 6c reveal differences in the fresh and spent $LaV_{0.03}Co_{0.97}O_3$ catalysts. The reduction to metallic Co (peak between 400–600 °C) in the spent catalyst is significantly higher than for the fresh catalyst. As also confirmed by XPS, the TPR profiles indicate that the spent catalyst is in a significantly reduced state after cyclohexane oxidation. The reduction can favor the exsolution of CoO during the reaction and, therefore, the reduction to metallic Co is enhanced in the TPR profile.[50] The initial consumption peak between 200–300 °C shows the primary reduction of Co^{3+} to Co^{2+} and is observed only for the fresh catalyst.[51,52] The absence of this feature in the spent catalyst points to a significant reduction of Co^{3+} to Co^{2+} during the reaction. As the particle size is also between 5-10 nm, the calculated degree of dispersion, which is the fraction of surface atoms, is roughly below 10%,[53] which in turn reveals that multiple layers below the surface are involved during catalysis.

As Figure 6d shows, the field-dependent magnetization at 5 and 300 K of the fresh and spent catalyst further confirms the changes in the catalyst during cyclohexane oxidation. In general, both catalysts exhibit paramagnetic behavior. The field-

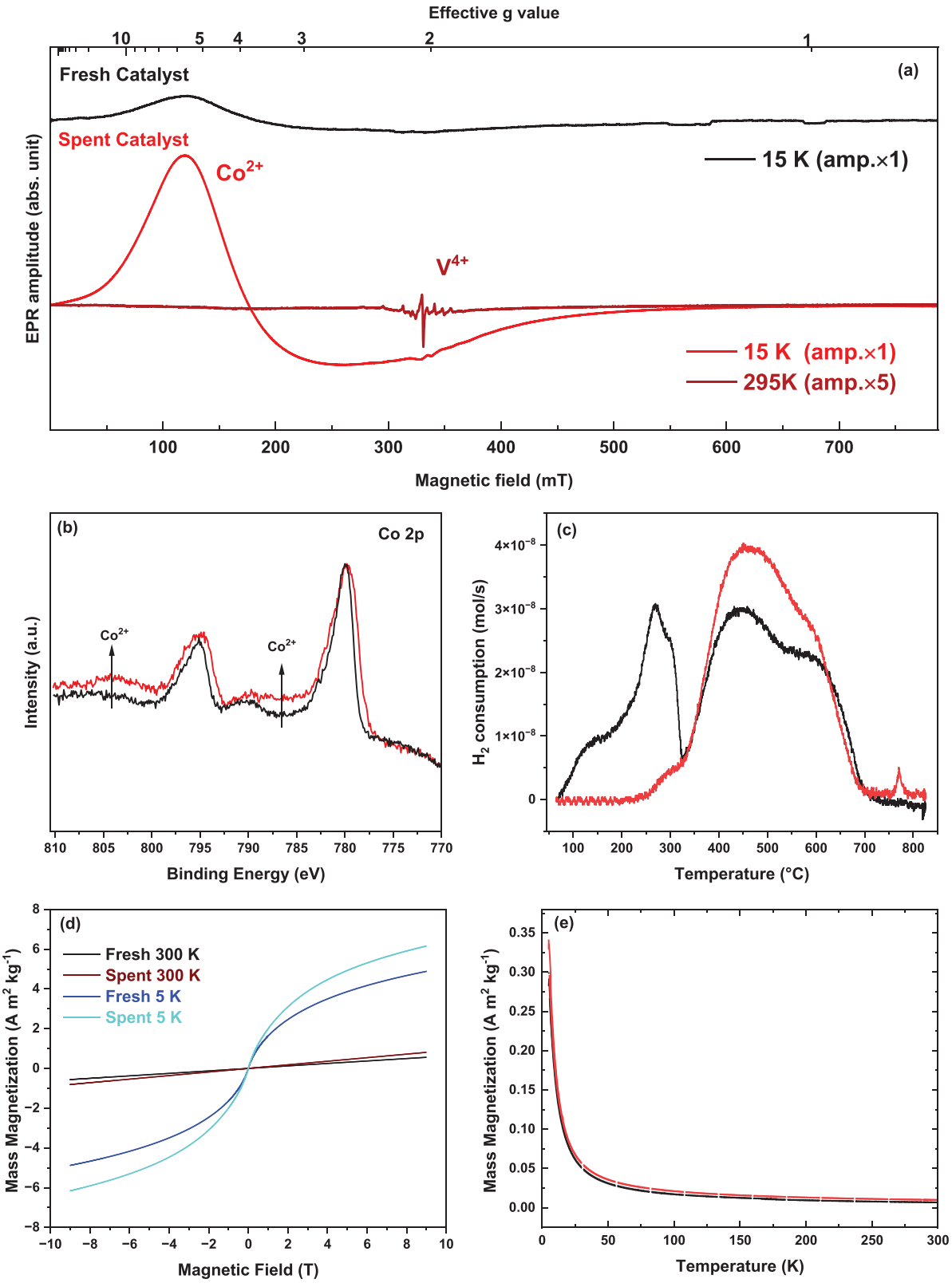

Figure 6. a) Solid-state EPR measurements of the fresh and spent $LaV_{0.03}Co_{0.97}O_3$ samples, b) Co 2p XP spectra (normalized), and c) H_2 TPR profiles of the fresh and spent $LaV_{0.03}Co_{0.97}O_3$ samples, d) magnetic field dependence of the mass magnetization of fresh and spent $LaV_{0.03}Co_{0.97}O_3$ at 5 K and 300 K, e) temperature-dependent magnetization of fresh and spent $LaV_{0.03}Co_{0.97}O_3$.

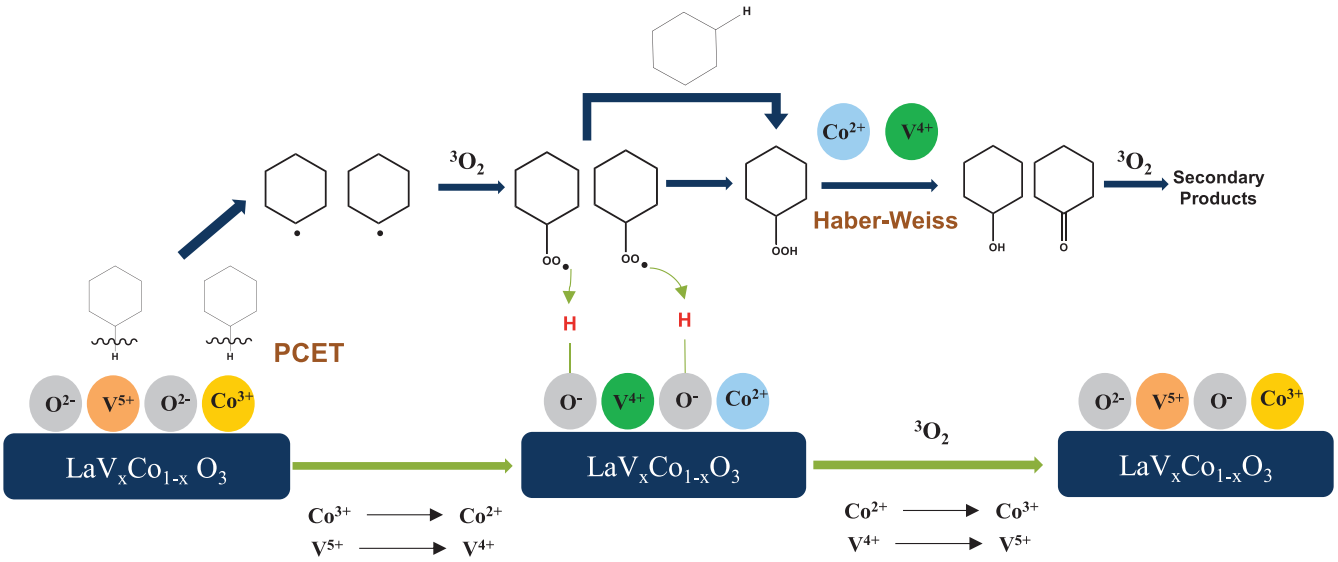

Figure 7. Reaction mechanism consisting of homolytic C-H breaking, reduction of the surface by PCET leading to CHHP decomposition via the Haber–Weiss reaction, and reoxidation by O_2.

dependent measurements, especially at 5 K, reveal a relatively higher magnetization of the spent catalyst. As indicated by the XPS, TPR, and EPR measurements, the partial reduction of the catalyst (e. g. diamagnetic Co^{3+} or V^{5+} to paramagnetic Co^{2+}or V^{4+}) alters its magnetic properties. Figure 6e shows the temperature-dependent magnetization, which, even though there are only minor differences, exhibits a slightly higher magnetization for the spent catalyst.

2.6. Mechanistic Considerations

In general, cyclohexane oxidation over La-based perovskites is assumed to occur via a partial surface reduction caused by the PCET process during C-H cleavage (initiation).[25] Figure 7 depicts the assumed PCET process occurring on the $LaV_xCo_{1-x}O_3$ surface during cyclohexane oxidation in more detail. Due to its strongly ionic nature, the La^{3+} coordination results in an increased electron density around the lattice oxygen. The C-H cleavage leads to the generation of $C_6H_{11}^{\bullet}$, an electron, and a proton. While the lattice oxygen accepts the proton, the higher-valent cations Co^{3+} and V^{5+} are reduced by the electron to the lower-valent states Co^{2+} and V^{4+}. Therefore, a partial reduction of the surface is assumed to occur as indicated by the characterization results obtained with the spent catalyst. The reduced cations Co^{2+} and V^{4+} then facilitate the CHHP decomposition via the Haber–Weiss cycle and are re-oxidized by molecular O_2. As shown in Figure S9b, V-doped $LaCoO_3$ has a superior activity in TBHP decomposition compared with $LaCoO_3$. Therefore, V as a dopant is also expected to improve the CHHP decomposition in cyclohexane oxidation. Figure S15 compares the selectivities of CHHP at similar conversion to demonstrate the influence of V in catalytic cyclohexane oxidation. While the blank reaction yielded a CHHP selectivity of 14.1%, adding $LaCoO_3$ as a catalyst further decomposed CHHP efficiently with a final selectivity of 8.7%. Upon V doping (x = 0.03), this was further lowered to 4.3%, indicating enhanced CHHP decomposition compared with $LaCoO_3$.

A significant formation of superoxide radical anions was identified by the EPR spin trap measurements. The electrons generated by the C-H cleavage can also be captured by the oxidant O_2, forming $O_2^{\bullet-}$, which may then be involved in the radical mechanism of cyclohexane oxidation. Further time-resolved studies based on spin trap EPR studies and advanced synchrotron-based characterization techniques are required to confirm such a radical pathway and to identify the oxidation state and local coordination of doped vanadium.

3. Conclusion

Spray flame-synthesized $LaV_xCo_{1-x}O_3$ nanoparticles with varying vanadium content were found to be active and selective in the liquid-phase oxidation of cyclohexane. Characterization of the as-synthesized catalysts using XRD confirmed phase-pure $LaV_xCo_{1-x}O_3$ nanoparticles up to x = 0.1. The beneficial effect of V doping led to an increasing cyclohexane conversion to 22.5% with 17.1% KA oil yield for x = 0.03. Kinetic investigations performed over $LaV_{0.03}Co_{0.97}O_3$ resulted in a cyclohexane reaction order of 1.0 and a low apparent activation energy of 44.8 kJ mol^{-1} due to the Co^{2+} fraction generated upon doping of higher-valent vanadium that has a superior activity in decomposing the cyclohexyl hydroperoxide (CHHP) intermediate. Reusability studies performed over three consecutive runs exhibited comparable performance, with maintenance of structural integrity confirmed by the XRD, Raman, HR-TEM, and leaching measurements. The ability of the catalyst to decompose the CHHP intermediate was studied using TBHP as a model hydroperoxide, showing that the spent catalyst evolved more O_2 than the fresh catalyst.

Radical scavenging experiments and spin trap EPR further confirmed a reaction-time-dependent free-radical mechanism

during cyclohexane oxidation, involving $C_6H_{11}OO^{\bullet}$, $C_6H_{11}O^{\bullet}$, $HO^{\bullet}$, $O_2^{\bullet-}$, and $C_6H_{11}^{\bullet}$. Examination of the spent catalyst using solid-state EPR confirmed a significantly increased Co^{2+} content and the formation of V^{4+} during cyclohexane oxidation. Further characterization of the spent catalyst using XPS, H_2 TPR, and magnetometry confirmed the spent catalyst to be in a more reduced state compared with the fresh catalyst. A plausible reaction mechanism based on an initial PCET reaction was proposed, where lattice oxygen acts as a proton acceptor and the higher-valent metal cations Co^{3+} and V^{5+} act as electron acceptors during C-H homolysis. Then, the lower-valent cations Co^{2+} and V^{4+} participate in a Haber-Weiss cycle, decomposing the CHHP intermediate, followed by their reoxidation by O_2.

4. Experimental Section

4.1. Catalyst Synthesis

Nanomaterials applied for oxidation reaction tests were obtained by spray-flame synthesis. The setup consists of an in-house developed spray-flame reactor and a standardized SpraySyn[54] nozzle, which is described in preceding publications.[55,56] The liquid precursor is composed of metal acetates, $La(CH_3CO_2)_3{\cdot}1.5\ H_2O$ (Alfa Aesar, 99.9%), $Co(CH_3CO_2)_2{\cdot}4\ H_2O$ (Sigma-Aldrich, reagent grade), and acetyl-acetonate $V(C_5H_7O_2)_3$ (Sigma-Aldrich, 97%), which were dissolved in a mixture (35:65 vol.%) of ethanol and 2-ethylhexanoic acid at 70 °C. A precursor with a total metal ion concentration of 0.2 mol/L was transferred with a constant feed rate of 2 mL/min to the nozzle of the SpraySyn burner, where the spray was formed. In the nozzle, the precursor was brought into contact with the dispersion gas, a stream of mixed gases (1 slm CH_4, 4.8 slm O_2), and formed a fine spray. To make sure that the flame is stable and to avoid fluctuations in ignition, a premixed methane/oxygen flat flame (2 slm CH_4, 16 slm O_2) on a sintered bronze plate was used. The pilot flame was stabilized using a sheath gas flow (140 slm compressed air). An additional gas flow (240 slm compressed air) was used downstream of the flame for quenching and controlling the off-gas temperature. The particles were precipitated on a PTFE-coated fiber membrane filter and collected after synthesis was completed.

4.2. Catalytic Cyclohexane Oxidation and Spin Trap Studies

The reaction was carried out using a Parr stainless steel high-pressure 4560 reactor equipped with an impeller-based stirring. Initially, the experiments were optimized at 1.00 mol/L of cyclohexane in 40 mL acetonitrile with biphenyl as the internal standard. Directly after transferring, the reactor was sealed and pressurized using molecular oxygen. Following the O_2 flushing three times, the reactor was heated to the desired temperature. The stirring followed once the set temperature was achieved. The samples were taken at 1, 2, 4, and 6 h of the reaction with two vials per withdrawal. The one was treated with previously weighed triphenylphosphine to reduce the CHHP to cyclohexanol. The CHHP was quantified by subtracting the cyclohexanol amount from the reduced and non-reduced sample. Kinetic investigations were carried out by varying reaction parameters such as reaction temperature, O_2 pressure, initial cyclohexane concentration, and stirring speed. The reaction parameters were then optimized at 130 °C, 1.00 mol/L cyclohexane, 15 bar O_2, and 600 rpm.

The quantification of the reaction mixture was carried out using a 7820-A gas chromatograph from Agilent Technologies equipped with a DB-XLB column (30 m*180 µm*0.18 µm). The following set parameters were used: injection volume, 1 µL; split flow, 9.98 mL/min; He flow, 0.4 mL/min; inlet temperature, 260 °C; split ratio, 1:25; initial pressure, 1.25 bar. Initially, an oven temperature of 80 °C and a hold time of 3 min were applied, and thereafter the temperature was increased to 140 °C with a heating rate of 17 °C without hold. Finally, an end temperature of 300 °C was achieved with a heating rate of 20 °C and 3 min hold time. The relative sensitivity factor (RSF) of biphenyl was set to 1 for quantification using peak area values. The following equations were used to determine the conversion, yield, and carbon balance. X_i is conversion; $n_{i,0}$ and n_i are the initial and final cyclohexane concentrations, respectively; Y_p is the product yield; n_p is the amount of product formed.

$$\text{Carbon Balance}\ (\%) = \frac{\text{Sum of Yields}\,(\%)}{\text{Conversion}\ (\%)} \times 100 \tag{1}$$

$$X_i = \frac{n_{i,0} - n_i}{n_{i,0}} \tag{2}$$

$$Y_p = \frac{n_p}{n_{i,0}} \tag{3}$$

Reusability studies were performed via three consecutive reactions with standard reaction conditions: 130 °C, 1.00 mol/L cyclohexane, 25 mg catalyst, 15 bar O_2, 600 rpm, and 6 h. Each run followed a catalyst recovery by centrifugation, acetonitrile wash, and overnight drying at 120 °C. ICP-MS measurements were conducted using the reaction solution collected after each run. Measurements were performed using an iCAP RQ ASX-560 instrument, where the samples were diluted in ultrapure water (1:10) followed by filtration and acidification using 300 µL HNO_3.

EPR spin trap experiments were carried out using DMPO based on previous studies.[25] The standard procedure followed was mixing 1 mL of the reaction mixture with 1 mg of DMPO at the desired time interval. To remove the dissolved O_2 and to improve the spectral quality, Ar was bubbled for 60 s prior to the spectral accumulation. The samples were transferred to a tube (1.6*1.0 OD/ID mm) and then placed to a Bruker Magnettech ES5000 bench-top spectrometer. The following parameters were used: 332–342 mT (magnetic field); 0.05 mT (modulation amplitude); 9.46 GH_z (microwave frequency); 15 mW (microwave power). 60 scans were taken first, and the samples were kept in liquid nitrogen. Further steps followed a higher acquisition of 2000 scans to obtain a better signal-to-noise ratio. The recorded spectra were simulated using "EasySpin" from MATLAB with the function "garlic".

4.3. Catalytic Characterization

XRD measurements were conducted using a Bruker D8 DISCOVER with theta-theta geometry, Cu Kα radiation (λ = 0.15,406 nm, 40 kV, 40 mA), and an energy-dispersive LYNXEYE XE-T detector. Angles from 10° to 120° 2θ were measured with a step size of 0.02° and a time per step of 3.0 s. The instrument was further equipped with a motorized airscatter aperture above the sample holder. The samples were placed on Si single crystals, and the sample holders were rotated during the measurements at a rate of 5 min^{-1}. All measurements were conducted at room temperature and atmospheric pressure.

In preparation for BET measurements, about 50 mg of the samples were weighed and evacuated for 12 h at 200 °C. The measurement was performed in a NOVA 800 from AntonPaar in 9 mm

cells. The adsorbant used was 99.99 % N_2 for a 7-point measurement between 0.04 and 0.3 relative pressure.

Raman measurements were carried out using a LabRAM HR Evolution spectrometer (Horiba) equipped with a confocal microscope containing a 100 times magnification objective. A green laser (532 nm, 100 mW, Oxxius) was used for measurements at R.T. by applying 1% laser power for 300 s with 4 accumulations.

X-band cw EPR were acquired using a Bruker Elexsys E580 EPR spectrometer equipped with an MD-BGO3 resonator and an ESR 900 He cryostat at 15 K. The EPR spectra were recorded at 15 and 295 K with 2 mW microwave power, 1400 mT field sweep centered at 700 mT, a modulation amplitude of 0.7 mT, a time constant of 41.96 ms, a sweep time of 587 s, and a modulation frequency of 100 kHz.

H_2 TPR measurements were conducted using a stainless-steel U-tube reactor with a thermal conductivity detector. A pre-treatment of the catalyst in He at 400 °C for 1 h was followed by cooling to 60 °C. The measurements were then conducted using a gas mixture of 50 mL/min 4.69% H_2/Ar heated to 800 °C with a holding for 60 min and a heating rate of 5 K/min. The temperature was monitored using a thermocouple inside the reactor every 2 s.

Magnetometry measurements were carried out using a Quantum Design PPMS DynaCool vibrating sample magnetometer. M(H) curves recorded at 5 K and 300 K were used to analyze the field-dependent magnetization (±9 T up maximum field) while M(T) curves recorded by zero field cooled-field cooled (ZFC-FC) curves with a sweep rate of 3 K min^{-1} between 5 and 300 K under an applied magnetic field of 0.1 T to investigate temperature-dependent magnetization.

High-resolution TEM images were collected by utilizing a probe-side Cs-corrected Jeol JEM 2200FS field emission electron microscope operated at 200 kV acceleration voltage.

Supporting Information

The supporting information is available at free of charge via the internet at https://chemistry-europe.onlinelibrary.wiley.com/. XRD unit cell parameters, surface areas, catalytic screening, kinetic investigations, radical scavenging studies, reusability studies, TEM results, ICP-MS measurements, TBHP decomposition, XPS results.

Acknowledgments

The work was supported and funded by the Deutsche Forschungsgemeinschaft (DFG, German Research Foundation, project number - 388390466-TRR 247). The authors acknowledge the H_2 TPR measurements by Mrs. Noushin Arshadi (Laboratory of Industrial Chemistry, Ruhr University Bochum). The authors also gratefully acknowledge Patrick Diehl, M.Sc. (Laboratory of Industrial Chemistry, Ruhr University Bochum) for the XRD measurements. Dr. Markus Heidelmann (Interdisciplinary Center for Analytics on the Nanoscale (ICAN), University of Duisburg-Essen) is acknowledged for the HR-TEM measurements. The authors also thank Dr. Ulrich Hagemann (ICAN, University of Duisburg-Essen) for the XPS measurements. This work was supported by the "Center for Solvation Science ZEMOS" funded by the German Federal Ministry of Education and Research BMBF and by the Ministry of Culture and Research of North Rhine-Westphalia.

Open access funding enabled and organized by Projekt DEAL.

Conflict of Interests

The authors declare no conflict of interest.

Data Availability Statement

The data that support the findings of this study are available from the corresponding author upon reasonable request.

Keywords: Cyclohexane oxidation · Radical scavenging · Spin trap EPR studies · Superoxide radical anion

[1] M. A. Andrade, L. M. Martins, *Catalysts* **2020**, *10*, 2.
[2] L. Wang, S. Zhao, C. Liu, C. Li, X. Li, H. Li, Y. Wang, C. Ma, Z. Li, J. Zeng, *Nano Lett.* **2015**, *15*, 2875–2880.
[3] A. M. Meireles, D. C. S. Da Martins, *Polyhedron* **2020**, *187*, 114627.
[4] Sdjad.
[5] W. Yan, G. Zhang, J. Wang, M. Liu, Y.u Sun, Z. Zhou, W. Zhang, S. Zhang, X. Xu, J. Shen, X. Jin, *Front. Chem.* **2020**, *8*, 185.
[6] D. Pan, G. Li, Y. Su, H. Wei, Z. Luo, *Chin. J. Chem. Eng.* **2021**, *29*, 183–189.
[7] J. R. L. Smith, D. I. Richards, C. B. Thomas, M. Whittaker, *J. Chem. Soc., Perkin Trans. 2* **1992**, 605.
[8] J. R. L. Smith, D. I. Richards, C. B. Thomas, M. Whittaker, *J. Chem. Soc., Perkin Trans. 2* **1985**, 1677.
[9] A. Abutaleb, M. A. Ali, *Reviews in Chemical Engineering* **2022**, *38*, 769–797.
[10] S. Alini, P. BABINI, in *Handbook of Advanced Methods and Processes in Oxidation Catalysis* (Eds: D. Duprez, F. Cavani), Imperial College Press, London **2014**.
[11] P. J. Hermans, J. Peeters, *Chem. Eur. J.* **2007**, *13*, 754–761.
[12] I. Hermans, T. L. Nguyen, P. A. Jacobs, J. Peeters, *ChemPhysChem* **2005**, *6*, 637–645.
[13] I. Hermans, P. A. Jacobs, J. Peeters, *J. Mol. Catal. A: Chem.* **2006**, *251*, 221–228.
[14] E. F. J. Duynstee, J. L. J. P. Hennekens, *Recl. Trav. Chim. Pays-Bas* **1970**, *89*, 769–780.
[15] J. Li, X.u Li, Y. Shi, D. Mao, G. Lu, *Catal. Lett.* **2010**, *137*, 180–189.
[16] X. Song, J. Hao, Y. Bai, L. Han, G. Yan, X. Lian, J. Liu, *New J. Chem.* **2017**, *41*, 4031–4039.
[17] M. Sadiq, M. Khan, M. Numan, R. Aman, S. Hussain, M. Sohail Ahmad, S. Sadiq, M. Abid Zia, H. Ur Rashid, R. Ali, *J. Chem.* **2017**, *2017*, 1–8.
[18] A. Pokutsa, J. Le Bras, J. Muzart, *Kinet. Catal.* **2007**, *48*, 26–31.
[19] A. Kumar, G. S. Mishra, A. Kumar, *Transit. Met. Chem.* **2003**, *28*, 913–917.
[20] T. F. S. Silva, L. M. D. R. S. Martins, M. F. C. Guedes Da Silva, M. L. Kuznetsov, A. R. Fernandes, A. Silva, C.-J. Pan, J.-F.u Lee, B.-J. Hwang, A. J. L. Pombeiro, *Chem. Asian J.* **2014**, *9*, 1132–1143.
[21] C. Hettige, K. R. R. Mahanama, D. P. Dissanayake, *Chemosphere* **2001**, *43*, 1079–1083.
[22] E. Yuan, M. Gu, P. Jian, *Korean J. Chem. Eng.* **2020**, *37*, 1137–1148.
[23] C. Xu, L. Jin, X. Wang, Y. Chen, L. Dai, *Carbon* **2020**, *160*, 287–297.
[24] E. Muhumuza, P. Wu, T. Nan, L. Zhao, P. Bai, S. Mintova, Z. Yan, *Ind. Eng. Chem. Res.* **2020**, *59*, 21322–21332.
[25] A. Hareendran, M. Dreyer, T. Sato, N. Cosanne, C. L. Leroy, B. Peng, M. Behrens, A. Schnegg, M. Muhler, *Mol. Catal.* **2024**, *569*, 114615.
[26] J. Geiss, J. Büker, J. Schulte, B. Peng, M. Muhler, M. Winterer, *J. Phys. Chem. C* **2023**, *127*, 5029–5038.
[27] R. B. Wexler, G. S. Gautam, E. B. Stechel, E. A. Carter, *J. Am. Chem. Soc.* **2021**, *143*, 13212–13227.
[28] Z. Wei, M. Zhao, Z. Yang, X. Duan, G. Jiang, G. Li, F. Zhang, Z. Hao, *Proc. Natl. Acad. Sci. USA* **2023**, *120*, e2217148120.
[29] Z. Su, J. Wu, T. Song, L. Duan, P. Zhang, L. Sun, K. Fan, *J. Mater. Chem. A* **2025**, *13*, 2789–2800.

[30] T. A. Yamamoto, K. Wachi, M. Hara, K. Kamata, *ACS Appl. Mater. Interfaces* **2024**, *16*, 62244–62253.
[31] S. Wu, Z. Shi, F. Dong, X. Song, W. Han, W. Han, H. Zhang, X. Dong, Z. Tang, *J. Mater. Chem. A* **2025**, *13*, 7539–7553.
[32] H. Chang, E. Bjørgum, O. Mihai, J. Yang, H. L. Lein, T. Grande, S. Raaen, Y.i-A.n Zhu, A. Holmen, D.e Chen, *ACS Catal.* **2020**, *10*, 3707–3719.
[33] R. Wei, X. Bu, W. Gao, R. A. B. Villaos, G. Macam, Z.-Q. Huang, C. Lan, F.-C. Chuang, Y. Qu, J. C. Ho, *ACS Appl. Mater. Interfaces* **2019**, *11*, 33012–33021.
[34] X. Luo, L. Zhang, M. Guo, Z. Liu, D. Wu, D. Zhen, Y. Liu, *ACS Appl. Mater. Interfaces* **2022**, *14*, 50055–50067.
[35] A. Goldstein, A. Zandonà, *Ceramics* **2025**, *8*, 16.
[36] C. D. Daub, I. Zakai, R. Valiev, V.-T. Salo, R. B. Gerber, T. Kurtén, *Phys. Chem. Chem. Phys.* **2022**, *24*, 10033–10043.
[37] D. Lončarević, J. Krstić, J. Dostanić, D. Manojlović, Ž. Čupić, D. M. Jovanović, *Chem. Eng. J.* **2010**, *157*, 181–188.
[38] J. Büker, B. Peng, *Mol. Catal.* **2022**, *525*, 112367.
[39] B. Tuo, Z. Wang, Z. Ren, H. Zhang, X. Lu, Y. Zhang, S. Zang, Y. Song, *Energy Environ. Sci.* **2024**, *17*, 2945–2955.
[40] L.e Li, C. Hao, R. Zhai, W. He, C. Deng, *Fuel* **2023**, *331*, 125853.
[41] D. R. Cooper, N. M. Dimitrijevic, J. L. Nadeau, *Nanoscale* **2010**, *2*, 114–121.
[42] J. Büker, X. Huang, J. Bitzer, W. Kleist, M. Muhler, B. Peng, *ACS Catal.* **2021**, *11*, 7863–7875.
[43] M. von Piechowski, M.-A. Thelen, J. Hoigné, R. E. Bühler, *Ber Bunsenges Phys. Chem.* **1992**, *96*, 1448–1454.
[44] M. Popa, *Solid State Ionics* **2002**, *154-155*, 135–141.
[45] F. Bai, J. Schulwitz, T. Priamushko, U. Hagemann, A. Kostka, M. Heidelmann, S. Cherevko, M. Muhler, T. Li, *J. Catal.* **2024**, *438*, 115697.
[46] K. Wang, W. Li, J. Huang, J. Huang, G. Zhan, Q. Li, *J. Energy Chem.* **2021**, *53*, 9–19.
[47] P. Lommens, F. Loncke, P. F. Smet, F. Callens, D. Poelman, H. Vrielinck, Z. Hens, *Chem. Mater.* **2007**, *19*, 5576–5583.
[48] I. Nevjestić, H. Depauw, K. Leus, V. Kalendra, I. Caretti, G. Jeschke, S. van Doorslaer, F. Callens, P. van der Voort, H. Vrielinck, *ChemPhysChem* **2015**, *16*, 2968–2973.
[49] M. C. Biesinger, B. P. Payne, A. P. Grosvenor, L. W. Lau, A. R. Gerson, R. S. Smart, *Appl. Surf. Sci.* **2011**, *257*, 2717–2730.
[50] M. Radovic, S. A. Speakman, L. F. Allard, E. A. Payzant, E. Lara-Curzio, W. M. Kriven, J. Lloyd, L. Fegely, N. Orlovskaya, *J. Power Sources* **2008**, *184*, 77–83.
[51] N. Yigit, K. Föttinger, J. Bernardi, G. Rupprechter, *J. Catal.* **2025**, *443*, 115973.
[52] W. Xie, G. Xu, Y. Zhang, Y. Yu, H. He, *J. Hazard. Mater.* **2022**, *431*, 128528.
[53] W. Grünert, W. Kleist, M. Muhler, *Catalysis at Surfaces*, De Gruyter, Berlin **2023**.
[54] F. Schneider, S. Suleiman, J. Menser, E. Borukhovich, I. Wlokas, A. Kempf, H. Wiggers, C. Schulz, *Rev. Sci. Instrum.* **2019**, *90*, 085108.
[55] C. Schulz, T. Dreier, M. Fikri, H. Wiggers, *Proc. Combust. Inst.* **2019**, *37*, 83–108.
[56] S. Hardt, I. Wlokas, C. Schulz, H. Wiggers, *J. Nanosci. Nanotechnol.* **2015**, *15*, 9449–9456.

Manuscript received: July 25, 2025
Accepted manuscript online: August 21, 2025
Version of record online: ■■, ■■